abundance of Fe, estimated to be ≤2 nM (*26, 27*), and its very short resident time of $\tau_{Fe} \approx 30$ years (*28*).
11. D. J. Piepgras and D. J. Wasserburg, *Earth Planet. Sci. Lett.* **45**, 223 (1979).
12. F. von Blanckenburg, R. K. O'Nions, N. S. Belshaw, A. J. Gibb, J. R. Hein, *Earth Planet. Sci. Lett.* **141**, 213 (1996).
13. J. N. Christensen, A. N. Halliday, L. V. Godfrey, J. R. Hein, D. K. Rea, *Science* **277**, 913 (1997).
14. K. W. Burton, H. F. Ling, R. K. O'Nions, *Nature* **386**, 382 (1997).
15. R. K. O'Nions, M. Frank, F. von Blanckenburg, H. F. Ling, *Earth Planet. Sci. Lett.* **155**, 15 (1997).
16. B. C. Reynolds, M. Frank, R. K. O'Nions, *Earth Planet. Sci. Lett.* **173**, 381 (1999).
17. Samples of Fe-Mn crust were dissolved in 6 M HCl and then purified by ion-exchange chromatography with 100% yields for Fe. Iron isotope ratios were determined with a Nu Instrument MC-ICPMS, following techniques described in (*1*). The concentration variations between samples and standard were controlled to be less than 20%.
18. X. K. Zhu, R. K. O'Nions, Y. Guo, N. S. Belshaw, D. Rickard, *Chem. Geol.* **163**, 139 (2000).
19. The $^{57}Fe/^{54}Fe$ ratios of samples are expressed in $\varepsilon^{57}Fe$ units according to the following definition:

$$\varepsilon^{57}\mathrm{Fe} = \left(\frac{R_{\mathrm{sample}}}{R_{\mathrm{standard}}} - 1\right) \times 10{,}000$$

where R_{sample} and $R_{standard}$ are the measured $^{57}Fe/^{54}Fe$ ratios for the unknown sample and the IRMM-14 Fe isotope reference standard, respectively. The Fe isotope reference standard IRMM-14 is commercially available and certified by the Institute for Reference Materials and Measurement, European Commission Joint Research Centre.
20. Naturally occurring Pb has four isotopes with masses of 204, 206, 207, and 208 atomic mass units. Of these, ^{206}Pb and ^{207}Pb are produced by the decay of the long-lived isotopes ^{238}U and ^{235}U, and ^{208}Pb is produced by long-lived ^{232}Th. These radiogenic daughters augment the initial abundances of the Pb isotopes in the solar system. The ratios $^{206}Pb/^{204}Pb$, $^{207}Pb/^{204}Pb$, and $^{208}Pb/^{204}Pb$ evolve with time in the natural environment according to time-dependent changes in the ratios of U/Pb and Th/Pb.
21. Iron has four stable isotopes, ^{54}Fe, ^{56}Fe, ^{57}Fe, and ^{58}Fe, with approximate terrestrial abundances of 5.85, 91.75, 2.12, and 0.28%, respectively. The relative abundances of these isotopes are expected to fractionate according to thermodynamic and kinetic effects (*1–3, 29*).
22. W. Abouchami, S. J. G. Galer, A. Koschinsky, *Geochim. Cosmochim. Acta* **63**, 1489 (1999).
23. R. A. Duce and N. W. Tindale, *Mar. Chem.* **36**, 1715 (1991).
24. M. L. Wells, N. M. Price, K. W. Bruland, *Mar. Chem.* **48**, 157 (1995).
25. N. M. Price and F. M. M. Morel, *Met. Ions Biol. Syst.* **35**, 1 (1998).
26. J. Wu and E. A. Boyle, *Anal. Chim. Acta* **367**, 183 (1997).
27. K. S. Johnson, R. M. Gordon, K. H. Coale, *Mar. Chem.* **57**, 137 (1997).
28. J. M. Bewers and P. A. Yeats, *Nature* **268**, 595 (1977).
29. V. B. Polyakov, *Geochim. Cosmochim. Acta* **61**, 4213 (1997).
30. The authors are grateful to N. S. Belshaw for his expertise in mass spectrometry. The constructive comments by two anonymous reviewers are highly appreciated. This work has been supported by a grant from the Natural Environment Research Council.

22 October 1999; accepted 2 February 2000

Modulation of Hurricane Activity in the Gulf of Mexico by the Madden-Julian Oscillation

Eric D. Maloney and Dennis L. Hartmann

The Madden-Julian oscillation (MJO) is a large-scale episodic modulation of tropical winds and precipitation that travels eastward from Asia to America, with a characteristic repeat time of 30 to 60 days. Here it is shown that when MJO wind anomalies in the lower troposphere of the eastern Pacific are westerly, Gulf of Mexico and western Caribbean hurricane genesis is four times more likely than when the MJO winds are easterly. Accurate predictions of the MJO may lead to improved long-range forecasts of tropical cyclone activity.

The Gulf of Mexico coastal regions of the United States have a history of devastating hurricanes and tropical storms (*1*). The deadliest recorded hurricane to hit the United States, the Galveston (Texas) hurricane of 1900, claimed over 8000 lives (*2, 3*). The most intense recorded hurricanes ever to make U.S. landfall—the Florida Keys hurricane of 1935 and Hurricane Camille of 1969—were category 5 hurricanes on the Saffir-Simpson scale (*4, 5*) that ravaged coastal regions of the Gulf of Mexico. The climatologically warm waters of the Gulf of Mexico and the western Caribbean Sea provide an abundant energy source for intense storms during the Atlantic basin hurricane season of May to November (*6*). Increasing our ability to forecast tropical storms and hurricanes has much potential for reducing the loss of life and property associated with these storms.

Here it is shown that the MJO, or tropical intraseasonal oscillation, modulates tropical cyclone activity over the Gulf of Mexico and the western Caribbean Sea. The MJO is characterized by an oscillation in tropical convection and winds at intraseasonal time scales of 30 to 60 days (*7, 8*). Tropical convection, accompanied by wind anomalies, develops over the Indian Ocean and moves eastward toward the Pacific Ocean. Atmospheric circulation anomalies propagate eastward into the eastern Pacific Ocean, where they may be amplified through interactions with convection during the Northern Hemisphere summer season. The MJO causes alternating periods of westerly and easterly wind anomalies (*9*) over the eastern Pacific. Tropical cyclone activity in the Gulf of Mexico appears to vary strongly in association with these intraseasonal wind variations.

This analysis uses wind data at 850 millibars (mb) (about 1400 m above sea level) from National Centers for Environmental Prediction–National Center for Atmospheric Research reanalysis (*10*) during 1949–1997 in pentad (5-day mean) format. Only data from May to November are used, corresponding to the Atlantic basin hurricane season. The reliability of our MJO index in this report is subject to the assumption that the reanalysis product produces realistic winds over the eastern Pacific. A comparison with surface wind data from ship reports (*11*) indicates that the reanalysis wind product agrees reasonably well with observed surface winds in the eastern Pacific. Tropical cyclone records for the Atlantic Ocean are taken from the National Oceanic and Atmospheric Administration (NOAA)/National Weather Service (NWS)/Tropical Prediction Center (*6*).

The principal component (PC) of the first empirical orthogonal function (EOF) for the 850-mb zonal wind is used as a measure of eastern Pacific MJO variability (*12, 13*). The first EOF, or the pattern explaining the maximum amount of temporal variance in the spatial domain of interest, resembles a zonal jet structure over the eastern Pacific, centered near 10°N (*14*). The first PC gives the amplitude of the first EOF as a function of time. This EOF explains 36% of the variance over the eastern Pacific and is closely related to MJO wind variations that emanate from the Indian Ocean and western Pacific regions (*13, 15*). The wind anomalies associated with the leading EOF have been shown to propagate from much farther west, and the EOF amplitude varies with a strong intraseasonal 40- to 50-day rhythm (*13*).

A positive value of the index coincides with westerly wind anomalies over the eastern Pacific Ocean. The average 850-mb wind anomalies for those pentads when the index is 1 SD more or less than zero are plotted in Fig. 1. Only vectors significantly different from zero at the 90% confidence level using a t distribution are displayed. The positive composite consists of 325 pentads and the negative composite consists of 322 pentads. Westerly phases are characterized by wind anomalies with cyclonic vorticity (*16*) over the eastern Pacific and the Gulf of Mexico. Tropical cyclone formation is favored in regions of cyclonic low-level relative vorticity (*17, 18*). MJO easterly phases are characterized by anticy-

Department of Atmospheric Sciences, University of Washington, Seattle, WA 98195–1640, USA.

clonic wind anomalies over the eastern Pacific, Gulf of Mexico, and western Caribbean.

The strongest wind anomalies shown in Fig. 1 occur in the eastern Pacific west of the Central American highlands. Recent studies have described a modulation of eastern Pacific hurricane activity by the MJO as represented by this wind pattern (*13, 19, 20*). During westerly MJO phases, hurricane genesis in the eastern Pacific is over four times more likely than during easterly periods and tends to occur closer to the Mexican coast, thereby increasing the chances of hurricane landfall. Hurricane formation in the eastern Pacific is favored by low-level cyclonic vorticity anomalies, low-level convergence, low vertical wind shear, and the growth of eddy disturbances through barotropic conversion from the mean flow during MJO westerly wind periods (*13, 17–20*). Other studies have suggested that wave instabilities may be important to eastern Pacific hurricane development through reversals of the lower tropospheric potential vorticity gradient (*21, 22*).

Here we show a new result that hurricanes in the Gulf of Mexico and the western Caribbean are also strongly modulated by the MJO wind anomalies. This is somewhat surprising because the Gulf of Mexico is separated from the largest MJO wind anomalies by the high topography of Central America and Mexico and is much farther north than the largest wind anomalies. The apparent influence of the MJO on Gulf of Mexico hurricanes is important for people living along the U.S. Gulf Coast, because a large fraction of Gulf Coast hurricanes make landfall.

The tracks of tropical storms and hurricanes that have genesis points in the Atlantic Ocean or Gulf of Mexico to the west of 77.5°W during westerly and easterly MJO phases are shown in Fig. 2. Genesis occurs when a system achieves a maximum sustained wind speed of 34 knots (17 m s^{-1}). Tropical cyclone formation during westerly MJO periods outnumbers formation during easterly MJO periods by 50 to 14. Hurricane genesis during westerly phases outnumbers formation during easterly phases by 24 to 6. The number of cyclones making landfall in Gulf Coast states shows similar increases for storms having genesis during westerly periods. The enhancement of tropical cyclone genesis during westerly MJO periods accompanies cyclonic wind anomalies over the Gulf of Mexico and western Caribbean. The distribution of tropical cyclone genesis events versus magnitude of the index indicates a strong preference for Gulf of Mexico, western Caribbean, and western Atlantic (west of 77.5°W) tropical cyclones to form during westerly MJO events (Fig. 3) (*23*). Hurricanes that are of category 3 strength (*4*) or greater have an even greater preference to occur during westerly MJO events.

We now want to show that all Gulf of Mexico and western Caribbean tropical cyclones are modulated by the MJO and not just tropical cyclones that form in those regions. The positions of all Atlantic tropical storms and hurricanes during westerly and easterly MJO phases are shown in Fig. 4. Cyclone positions are reported four times daily. The figure verifies that all tropical cyclone activity, not just cyclone genesis (Fig. 2), is enhanced over the Gulf of Mexico and western Caribbean Sea during westerly MJO events.

Previous work on Atlantic and Gulf of Mexico hurricanes has examined the influence of El Niño/southern oscillation (ENSO) (*24–26*).

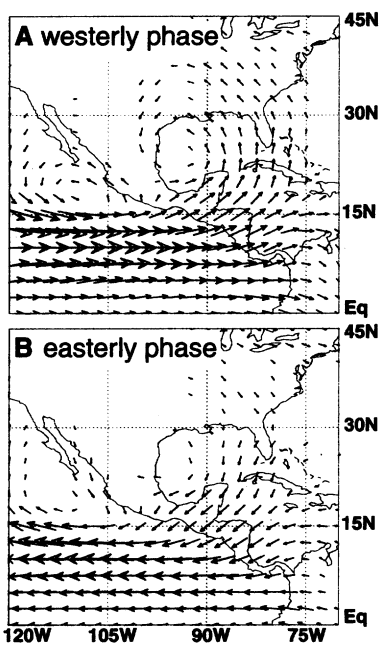

Fig. 1. Wind anomalies at 850 mb when the MJO index has a magnitude greater than 1 SD from zero. Positive (westerly, greater than 1 SD) (**A**) and negative (easterly, less than −1 SD) (**B**) phases are displayed. Only vectors significant at the 90% confidence level are displayed. Data span the period 1949–1997. Maximum wind vectors are 6.8 m s^{-1} over the eastern Pacific and 1.3 m s^{-1} over the Gulf of Mexico for the positive composite.

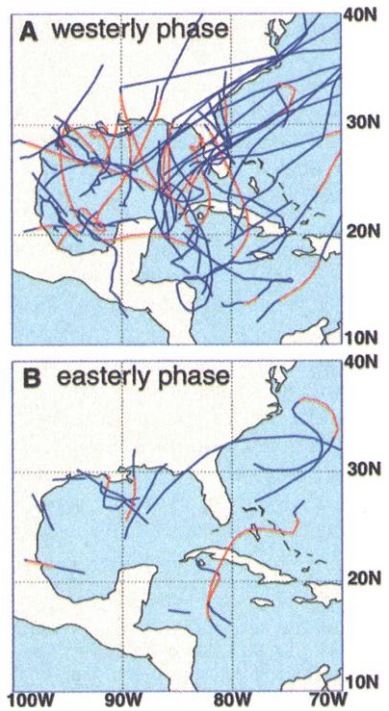

Fig. 2. Tracks of Gulf of Mexico, Caribbean Sea, and western Atlantic tropical cyclones that form to the west of 77.5°W when the MJO index has a magnitude greater than 1 SD from zero. Westerly (greater than 1 SD) (**A**) and easterly (less than −1 SD) (**B**) phases are displayed. Tropical storm tracks [winds between 34 and 64 knots (17 to 33 m s^{-1})] are plotted in blue. Hurricane tracks [winds greater than 64 knots (33 m s^{-1})] are plotted in red. Cyclone data span the period 1949–1997.

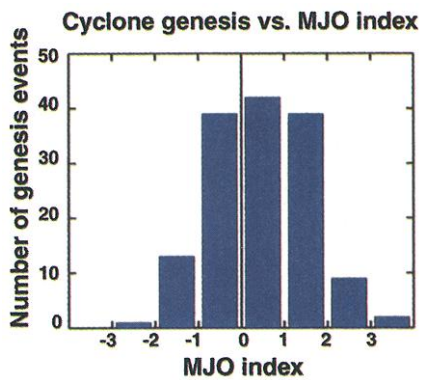

Fig. 3. Histogram of tropical cyclone genesis events for the western Atlantic, Caribbean Sea, and Gulf of Mexico to the west of 77.5°W as a function of the MJO index. Histogram categories are each 1 SD of the MJO index.

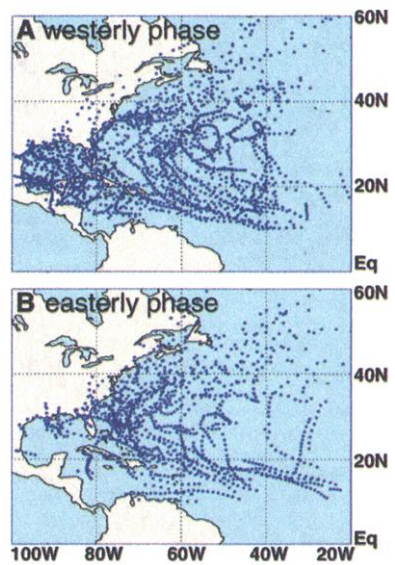

Fig. 4. Atlantic tropical storm and hurricane positions during westerly (greater than 1 SD) (**A**) and easterly (less than −1 SD) (**B**) MJO phases.

ENSO variations change the basic state wind fields over the Atlantic at interannual time scales, altering environmental conditions that may affect hurricane formation. This relationship offers some accuracy in predicting the number of hurricanes that may occur in a given year. Variations of tropical winds and precipitation on intraseasonal time scales associated with the MJO (*13, 19*) are at least as large as the interannual variations associated with ENSO, and they may offer the possibility of predicting which periods during the hurricane season are most likely to produce hurricanes. The slow evolution of the MJO may be forecast up to 2 weeks or more into the future (*27*). An accurate MJO forecast, combined with knowledge of how the MJO affects Gulf of Mexico and Caribbean hurricanes, can be used to improve extended-range forecasts of tropical cyclone activity. The tendency of tropical cyclones over the Gulf of Mexico and Caribbean to cluster in time (*28*) may be explained at least in part by the interactions with the MJO described here.

References and Notes

1. Tropical storm, winds 34 to 64 knots (17 to 33 m s^{-1}); hurricane, winds greater than 64 knots.
2. P. J. Hebert, J. D. Jarrell, M. Mayfield, *NOAA Technical Memorandum No. NWS-NHC-31* (NOAA, Washington, DC, 1993).
3. P. Lester, *The Great Galveston Disaster* (Marrow, St. John, New Brunswick, Canada, 1900).
4. Category 5 on the Saffir-Simpson scale corresponds to winds greater than 135 knots (155 mph, 69 m s^{-1}); category 3 corresponds to winds of 96 to 113 knots (111 to 130 mph, 49 to 58 m s^{-1}).
5. R. H. Simpson and H. Riehl, *The Hurricane and Its Impact* (Louisiana State University Press, Baton Rouge, 1981).
6. B. R. Jarvinen, C. J. Neumann, M. A. S. Davis, *NOAA Technical Memorandum No. NWS-NHC-22* (NOAA, Washington, DC, 1984).
7. R. A. Madden and P. R. Julian, *Mon. Weather Rev.* **122**, 814 (1994).
8. H. H. Hendon and M. L. Salby, *J. Atmos. Sci.* **51**, 2225 (1994).
9. Anomalies are defined as deviations from the mean annual cycle.
10. E. Kalnay *et al.*, *Bull. Am. Meteorol. Soc.* **77**, 437 (1996).
11. Data not shown.
12. J. E. Kutzbach, *J. Appl. Meteorol.* **6**, 791 (1967).
13. E. D. Maloney and D. L. Hartmann, unpublished data.
14. EOFs were computed for the region: Equator–30°N, 80°W–130°W. The first EOF is shown in (*13*).
15. The first PC has a zero-lag correlation of −0.6 with an MJO index in a previous study (*29*) that is dominated by western Pacific and Indian Ocean zonal wind variability.
16. Cyclonic circulations rotate in the same direction as the Earth, counterclockwise, as viewed from above in the Northern Hemisphere. Vorticity is a measure of the local rotation of a fluid.
17. W. M. Gray, *Meteorol. Atmos. Phys.* **67**, 37 (1998).
18. R. M. Zehr, *NOAA Technical Report No. NESDIS 61* (NOAA, Washington, DC, 1992).
19. E. D. Maloney and D. L. Hartmann, unpublished data.
20. D. L. Hartmann and E. D. Maloney, unpublished data.
21. J. Molinari, D. Knight, M. Dickinson, D. Vollaro, S. Skubis, *Mon. Weather Rev.* **125**, 2699 (1997).
22. R. N. Ferreira and W. H. Schubert, *J. Atmos. Sci.* **54**, 261 (1997).
23. The MJO index (the first PC) was normalized to unit variance for use in this figure. Positive values of the index correspond to westerly wind periods. The MJO index has zero mean and includes 1035 positive pentads and 1119 negative pentads. The number of genesis events during westerly periods of amplitude greater than one is significantly higher than the number during easterly periods of the same amplitude at the 95% confidence level.
24. W. M. Gray, *Mon. Weather Rev.* **112**, 1649 (1984).
25. C. W. Landsea, G. M. Gray, P. W. Mielke Jr., K. J. Berry, *Weather* **49**, 273 (1994).
26. M. C. Bove, J. J. O'Brien, J. B. Eisner, C. W. Landsea, X. Nie, *Bull. Am. Meteorol. Soc.* **79**, 2477 (1998).
27. D. E. Waliser, C. Jones, J.-K. E. Schemm, N. E. Graham, *J. Climate* **12**, 1918 (1999).
28. W. M. Gray, in *Meteorology over the Tropical Oceans*, D. B. Shaw, Ed. (Royal Meteorological Society, Bracknell, UK, 1979), pp. 155–218.
29. E. D. Maloney and D. L. Hartmann, *J. Climate* **22**, 2387 (1998).

30. Supported by the Climate Dynamics Program of the National Science Foundation under grant ATM-9873691.

3 December 1999; accepted 2 February 2000

Contribution of Increasing CO_2 and Climate to Carbon Storage by Ecosystems in the United States

David Schimel,[1]* Jerry Melillo,[2] Hanqin Tian,[2]* A. David McGuire,[3] David Kicklighter,[2] Timothy Kittel,[4] Nan Rosenbloom,[4] Steven Running,[5] Peter Thornton,[5] Dennis Ojima,[6] William Parton,[6] Robin Kelly,[6] Martin Sykes,[7] Ron Neilson,[8] Brian Rizzo[9]

The effects of increasing carbon dioxide (CO_2) and climate on net carbon storage in terrestrial ecosystems of the conterminous United States for the period 1895–1993 were modeled with new, detailed historical climate information. For the period 1980–1993, results from an ensemble of three models agree within 25%, simulating a land carbon sink from CO_2 and climate effects of 0.08 gigaton of carbon per year. The best estimates of the total sink from inventory data are about three times larger, suggesting that processes such as regrowth on abandoned agricultural land or in forests harvested before 1980 have effects as large as or larger than the direct effects of CO_2 and climate. The modeled sink varies by about 100% from year to year as a result of climate variability.

Recent analyses of the global carbon cycle suggest a significant role for terrestrial uptake of CO_2 in the overall budget (*1–4*). Analyses of atmospheric CO_2 have persistently suggested that this terrestrial uptake is largest in the Northern Hemisphere (*2, 3*), and one atmospheric analysis suggests that the United States may play a disproportionate role (*2*). Currently, a number of phenomena contribute to enhanced carbon uptake by ecosystems, including CO_2 fertilization of photosynthesis, climate, nitrogen deposition, recovery from historical land use, and erosion/sedimentation (*4–6*). Although preliminary attempts have been made to partition the terrestrial sink among these processes globally, this quantification is currently extremely crude. It is essential to understand the mechanisms controlling carbon exchange today as a basis for prediction and management interventions (*7*).

Here we present results from the Vegetation/Ecosystem Modeling and Analysis Project (VEMAP) aimed at understanding the contribution of ecosystem physiological mechanisms to terrestrial sinks in the conterminous United States during the period 1980–1993. Specifically, we consider how changes in climate and CO_2 concentration affect ecosystem physiology. Three ecosystem models [Biome-BioGeochemical Cycles (Biome-BGC), Century, and the Terrestrial Ecosystem Model (TEM)] that dynamically calculate net carbon storage at a 0.5° × 0.5° resolution (*8*) were used. All three models simulated changes to soil and vegetation carbon in natural ecosystems. Century simulated both natural and simulated agricultural ecosystems. To compute complete regional car-

[1]Max-Planck-Institute for Biogeochemistry, Postfach 10 01 64, D-07701 Jena, Germany. [2]The Ecosystems Center, Marine Biological Laboratory, Woods Hole, MA 02543, USA. [3]U.S. Geological Survey, Alaska Cooperative Fish and Wildlife Research Unit, University of Alaska, Fairbanks, AK 99775–7020, USA. [4]National Center for Atmospheric Research, P.O. Box 3000, Boulder, CO 80307–3000, USA. [5]University of Montana, Missoula, MT 59812, USA. [6]NREL, Colorado State University, Fort Collins, CO 80523–1499, USA. [7]Plant Ecology, Lund University, Ekologihuset 223 62 Lund, Sweden. [8]U.S. Department of Agriculture, Forest Service, Oregon State University, Forest Science Laboratory, 3200 Southwest Jefferson Way, Corvallis, OR 97333, USA. [9]Department of Environmental Sciences, University of Virginia, Charlottesville, VA 22903, USA.

*To whom correspondence should be addressed. E-mail: dschimel@bgc-jena.mpg.de and htian@mbl.edu